

Very rapid cooling of the energetic pyroclastic density currents associated with the 5 November 2010 Merapi eruption (Indonesia)

M. Trolese, G. Giordano, J. -C. Komorowski, S. F. Jenkins, P. J. Baxter, N. Cholik, P. Raditya, S. Corrado

▶ **To cite this version:**

M. Trolese, G. Giordano, J. -C. Komorowski, S. F. Jenkins, P. J. Baxter, et al.. Very rapid cooling of the energetic pyroclastic density currents associated with the 5 November 2010 Merapi eruption (Indonesia). Journal of Volcanology and Geothermal Research, 2018, 358, pp.1-12. 10.1016/j.jvolgeores.2018.06.004 . insu-03589348

HAL Id: insu-03589348

https://insu.hal.science/insu-03589348

Submitted on 25 Feb 2022

HAL is a multi-disciplinary open access archive for the deposit and dissemination of scientific research documents, whether they are published or not. The documents may come from teaching and research institutions in France or abroad, or from public or private research centers.

L'archive ouverte pluridisciplinaire **HAL**, est destinée au dépôt et à la diffusion de documents scientifiques de niveau recherche, publiés ou non, émanant des établissements d'enseignement et de recherche français ou étrangers, des laboratoires publics ou privés.

This document is downloaded from DR-NTU (https://dr.ntu.edu.sg)
Nanyang Technological University, Singapore.

Very rapid cooling of the energetic pyroclastic density currents associated with the 5 November 2010 Merapi eruption (Indonesia)

Trolese, M.; Giordano, G.; Komorowski, J. C.; Jenkins, Susanna F.; Baxter, P. J.; Cholik, N.; Raditya, P.; Corrado, S.

2018

Trolese, M., Giordano, G., Komorowski, J. C., Jenkins, S. F., Baxter, P. J., Cholik, N., . . ., Corrado, S. (2018). Very rapid cooling of the energetic pyroclastic density currents associated with the 5 November 2010 Merapi eruption (Indonesia). Journal of Volcanology and Geothermal Research, 358, 1-12. doi:10.1016/j.jvolgeores.2018.06.004

https://hdl.handle.net/10356/139833

https://doi.org/10.1016/j.jvolgeores.2018.06.004

© 2018 Elsevier B.V. This paper was published in Journal of Volcanology and Geothermal Research and is made available with permission of Elsevier B.V.

Downloaded on 25 Feb 2022 23:21:48 SGT

Contents lists available at ScienceDirect

Journal of Volcanology and Geothermal Research

journal homepage: www.elsevier.com

Very rapid cooling of the energetic pyroclastic density currents associated with the 5 November 2010 Merapi eruption (Indonesia)

M. Trolese[a,*], G. Giordano[a], J.-C. Komorowski[b], S. Jenkins[c], P.J. Baxter[d], N. Cholik[e], P. Raditya[e], S. Corrado[a]

[a] Dipartimento di Scienze, Sezione di Geologia, Università degli Studi Roma Tre, L.go S. Leonardo Murialdo 1, 00146 Roma, Italy
[b] Equipe Systèmes Volcaniques, Institut de Physique du Globe de Paris, Université Sorbonne Paris Cité, CNRS UMR-7154, Université Paris Diderot, Paris, France
[c] Earth Observatory of Singapore, Asian School of the Environment, Nanyang Technological University, Singapore 639798, Singapore
[d] Department of Public Health and Primary Care, University of Cambridge, Institute of Public Health, Robinson Way, Cambridge CB2 0SR, UK
[e] BPPTK (Balai Penyelidikan dan Pengembangan Tekonologi Kegunungapian), Yogyakarta, Indonesia

ARTICLE INFO

Article history:
Received 2 March 2018
Received in revised form 10 May 2018
Accepted 3 June 2018
Available online xxx

Keywords:
Merapi volcano
Pyroclastic density current
Charcoal reflectance
Emplacement temperature
Rapid cooling
Volcanic hazards

ABSTRACT

Understanding the thermal behavior of pyroclastic density currents (PDCs) is crucial for forecasting impact scenarios for exposed populations as it affects their lethality and destructiveness. Here we report the emplacement temperatures of PDC deposits produced during the paroxysmal explosive eruption of Merapi (Central Java) on 5 November 2010 based on the reflectance of entombed charcoal fragments. This event was anomalously explosive for Merapi, and destroyed the summit dome that had been rapidly growing, with partial collapses and associated PDCs, since October 26. Results show mean reflectance values mainly between 0.17 and 0.41. These new data provide a minimum temperature of the flow of 240–320 °C, consistent with previous estimations determined from independent field, engineering, and medical observations published in the literature for this eruption. A few charcoal fragments recorded higher values, suggestive of temperatures up to 450 °C, and we suggest that this is due to the thermal disequilibrium of the deposits, with larger block-size clasts being much hotter than the surrounding ash matrix. Charring temperatures show no major differences between proximal and distal PDC deposits and are significantly lower than those that may be associated with a fast growing dome dominated by dense and vitric non-vesicular rocks. We therefore infer that the decrease in temperature from that at fragmentation (>900 °C) occurred in the very initial part of the current, <2 km from source. We discuss possible processes that allow the very fast cooling of these energetic PDCs, as well as the conservative thermal behavior shown during the depositional phase, across the entire depositional area.

© 2017.

1. Introduction

The last major eruptive sequence of Merapi volcano, in Indonesia, began on 26 October and ended on 23 November 2010 (Surono et al., 2012). During this period, the activity was mostly characterized by recurrent rapid lava-dome growth and collapses, accompanied by numerous pyroclastic density currents (PDCs; ~~also~~ referred to as block-and-ash flow) that threatened the local settlements up to 15 km from the crater (Surono et al., 2012; Cronin et al., 2013; Jenkins et al., 2013; Komorowski et al., 2013; Charbonnier et al., 2013; Genareau et al., 2015). On 5 November 2010, a series of paroxysmal dome explosions and collapses generated several PDCs that inundated an area of 22 km^2, depositing ~5×10^6 m^3 of material (Komorowski et al., 2013). Despite the small volume of the eruptive products in comparison to other climactic phases, this event represents the most disastrous volcanic eruption observed at Merapi since 1872, being responsible for >200 fatalities and a massive destruction of buildings and trees (Jenkins et al., 2013; Baxter et al., 2017). The topography-mantling PDCs associated with this paroxysmal phase flowed down the southern flank of the volcano for 8.4 km crossing over transverse topographic ridges up to 245 m high, whereas co-genetic valley-confined PDCs continued propagating in the Gendol drainage reaching 15.5 km and producing concentrated overspills and dilute detached PDCs (Komorowski et al., 2013; Fig. 1).

The PDCs felled many trees in densely vegetated areas, the orientation of which was important for determining the flow dynamics. Through an extensive study of satellite imagery ~~and fieldwork,~~ Komorowski et al. (2013) reconstructed the complex flow direction pattern of the 5 November PDCs as a result of their interaction with a marked topography. They argue that the strongly directional tree blowdown and the distinctive bipartite stratigraphy of the topography-mantling PDC deposits, which are characterized by a lower coarse-grained, fines-poor massive and chaotic unit overlain by a finer-grained, fines-rich laminar to low angle cross-stratified unit, are characteristic features shared with other historical blast deposits, suggesting that the paroxysmal 5 November event was also a laterally-directed blast-like explosion. Moreover, Jenkins et al. (2013) used the evidence of damage to trees and structures, and the transport of boulders and debris, to derive the dynamic pressure evolution across the

* Corresponding author.
Email address: matteo.trolese@uniroma3.it (M. Trolese)

https://doi.org/10.1016/j.jvolgeores.2018.06.004
0377-0273/ © 2017.

UNCORRECTED PROOF

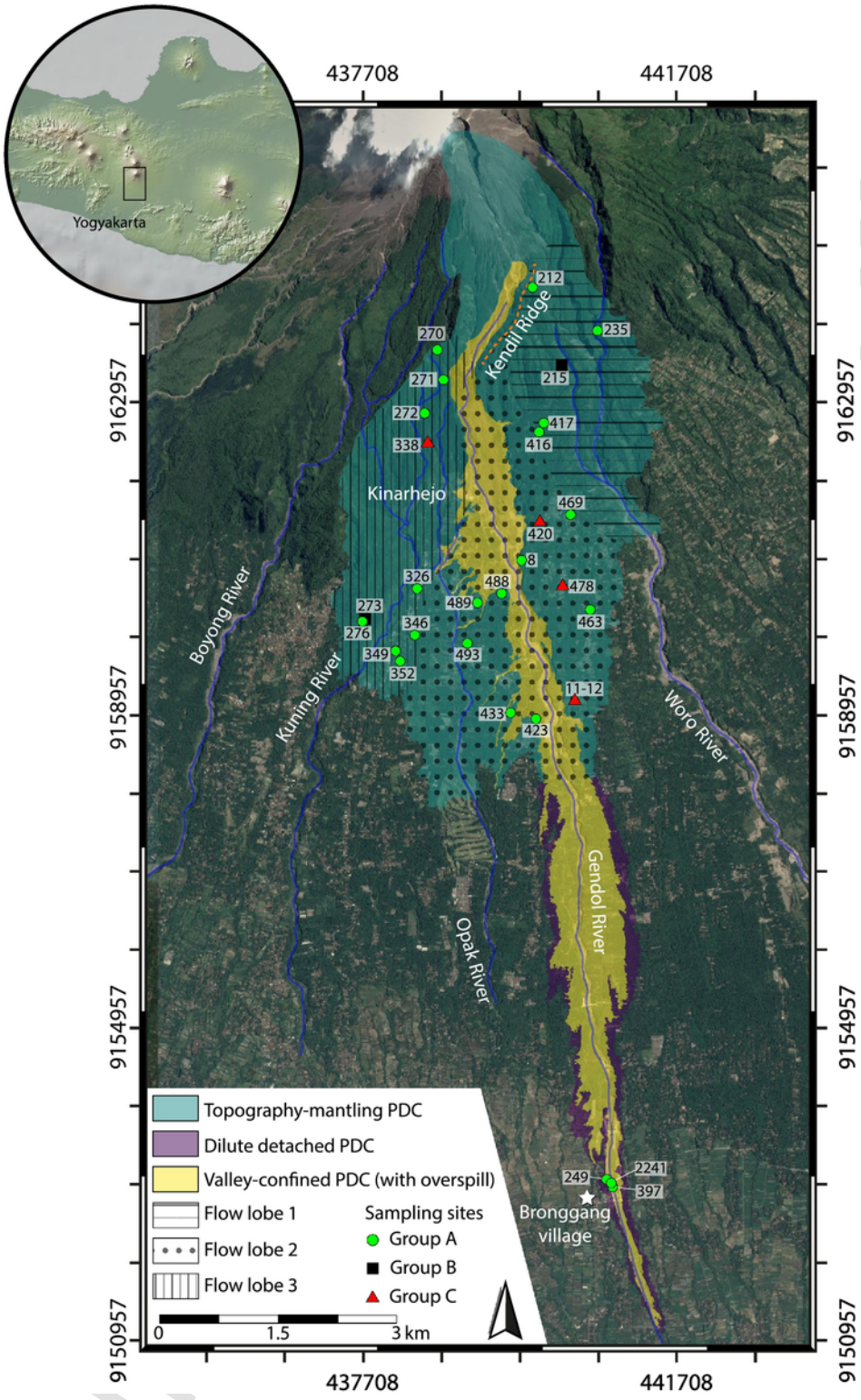


Fig. 1. Map showing the distribution of PDC deposits from the 5 November 2010 eruption at Merapi (simplified from Komorowski et al., 2013), and the sites sampled in this study (colors refer to the groups as defined by charcoal reflectance data, see Fig. 3). The inset box indicates the location of Merapi volcano in Central Java. The flow lobes (1 to 3) correspond to PDC-1, PDC-2 and PDC-3 in Komorowski et al. (2013); Fig. 3, b), respectively.

impact area of the topography-mantling PDCs, which were able to exert significant dynamic pressure (≥10 kPa) over distances of 5–6 km from the crater, despite their unconfined setting. Other studies have also used the damage to trees to infer velocities (and hence dynamic pressures) of other historical Merapi eruptions (Clarke and Voight, 2000; Kelfoun et al., 2000). Cronin et al. (2013) interpreted

the energetic event of 5 November as extremely hot and mobile block-and-ash flows generated by the collapse of a very hot and highly gas-charged dome, which were able to develop several decoupled dilute currents.

The PDC deposits associated with the Merapi 2010 paroxysm were also sufficiently hot to char most of the vegetation entombed along their extent. Experimental studies have shown that during the charcoalification process, the reflectance of charcoal increases with temperature (Correia et al., 1974; Scott and Jones, 1991; Scott and Glasspool, 2007). Even though reflectance could also increase at a given temperature with time, it stabilized after exposure >24 h (Scott and Glasspool, 2005). Thus, reflectance can be used as an indicator of the charring temperature of specimens embedded within PDC deposits. Despite its potential, the study of charcoal fragments has been adopted to determine the emplacement temperature of only few historical PDC deposits, including pyroclastic deposits at Soufrière Hills (325–525 °C, Scott and Glasspool, 2005; 300–425 °C, Scott et al., 2008), Taupo (269–398 °C, Hudspith et al., 2010), Vesuvius (240–370 °C, Caricchi et al., 2014) and Fogo (330–460 °C, Pensa et al., 2015). Laboratory studies have shown that reflectance measurements of charcoal can give precise information about the temperature of formation over a wide range of values, from 200 to >1100 °C, providing a broad range of geological applications (Ascough et al., 2010; McParland et al., 2009; Scott and Glasspool, 2005; Scott and Jones, 1991). A systematic exploration of the thermal state of PDCs (and its spatial and temporal variation) provides important insights into the flow dynamics, and enhances our ability to mitigate potential future hazards. However, our knowledge about how quickly the heat is exchanged between the pyroclastic mixture and the external environment is still limited. Estimated emplacement temperatures of PDCs of the recent activity at Merapi have been obtained using different types of proxies. In particular, the use of melting plastics has been adopted to infer the temperature of dilute PDCs emplaced during the 1994 eruption (<200 °C, Voight and Davis, 2000), and the 2006 eruption (<165 °C, Charbonnier and Gertisser, 2008). Jenkins et al. (2013) and Baxter et al. (2017) estimated low temperatures (200–300 °C) for the PDCs emplaced on 5 November both in proximal and distal localities. They used different strands of evidence, such as photographs and eyewitness accounts of thermal injuries in injured and deceased victims, building damages and field observations (i.e. heat effects on man-made objects and vegetation) to show that communities situated along the Gendol river at about 12 km from the crater and invaded by dilute detached PDCs, sustained low dynamic pressures but sufficiently high temperatures to cause injuries and fatalities (Baxter et al., 2017). However, the high extrusion rate (~25 $m^3 s^{-1}$; Pallister et al., 2013) of the new dome that collapsed on 5 November (which was built between 2 and 4 November), its dense non-vesicular texture and significant internal overpressure (Komorowski et al., 2013) suggest that it had experienced limited cooling and degassing and that it was very hot at that time (Cronin et al., 2013) providing a large supply of thermal energy for the associated PDCs. Hence, this raises the important question of determining what is the dominant process, between the source and the transport system of the PDCs, that was responsible for the sudden temperature drop recorded by previous studies. We address this question by investigating the spatial variation of the charring temperature of plant materials that were preserved within the PDC deposits of 5 November 2010, with the aim to characterize and inform the mechanisms for PDC transport and heat transfer with the external environment.

2. Material and methods

Several samples of charred material were collected from 29 sites in 2010 and 2011 (Fig. 1; Table 1). Samples from the topography-mantling PDC deposits were taken from depositional unit U1, interpreted by Komorowski et al. (2013) to be related to the most energetic explosion of the 2010 paroxysmal activity. This paroxysmal event corresponds to the third explosion of stage 4 in Komorowski et al. (2013), to phase 3 in Charbonnier et al. (2013) and to the end of phase 3 in Cronin et al. (2013). The reader may refer to these papers for detailed information on deposit characteristics. We provide here a brief description of the main features of the studied deposits. Unit U1 consists of two layers (L1 and L2) which were both deposited over similar areas, with a combined thickness that ranges from 150 cm in proximal areas to 1 cm at the final PDC runout. Charcoal fragments were generally sampled near the base or the middle of the thickness of the lower layer L1, which is a poorly sorted, massive to crudely stratified and fines-depleted layer (Fig. 2; Table 1). Layer L1 is rich in very dense and angular, vitric juvenile andesite clasts (>95% by count), and represents the coarsest layer with a maximum juvenile clast size of ~20 cm and median particle diameter between −4 and 1 ϕ (16 mm – 0.5 mm; see Fig. 13 of Komorowski et al., 2013). It varies locally in lithofacies, and pinches and swells as a result of topographic changes, reaching maximum thicknesses of 1.5 m around the Gendol river and 1 m on ridge tops within 4 km from the vent. In the absence of layer L1, charcoal fragments were sampled from the base of the upper layer L2 (Fig. 2; Table 1), which is a well sorted, fines-rich, matrix-supported layer mostly composed by the same juvenile material of L1 (80–95% by count; Komorowski et al., 2013). The median grain size of L2 varies from −0.5 to 3.5 ϕ (1.4 mm − 8 × [illegible] mm) with a maximum clast diameter of ~6 cm (see Fig. 13 of Komorowski et al., 2013). Layer L2 ranges from massive to strongly stratified, and forms a relatively continuous landscape-mantling veneer deposit. Its thickness varies from 50 cm in proximal areas to ~1 cm at about 8.5 km distance. In contrast with L1, L2 thickens and thins primarily due to small-scale variations of the topography, such as hollow depressions, boulders and tree stumps, and rarely due to major topographic features such as river valleys. The relationship between L1 and L2 is usually gradational, but locally their interface is abrupt. Degassing pipes are often present above the charred vegetation incorporated within L1 and L2. The whole U1 is generally covered by a second depositional unit (U2), which is related to another large explosion of the dome that occurred shortly after the main explosion (Komorowski et al., 2013). A pinkish accretionary lapilli ashfall unit overtops both these units.

Samples from the valley-confined facies of the 5 November PDCs were collected at the base of deposits that completely filled the Gendol channel near the village of Bronggang, at ~13 km from the summit (Fig. 1). These block-rich, massive and poorly sorted deposits are formed by at least two eruptive units, contemporaneous and co-genetic with the two main depositional units U1 and U2 (Charbonnier et al., 2013; Komorowski et al., 2013). They consist mainly of dense juvenile clasts similar to those of U1 and U2, with maximum clast sizes of 1–[illegible] and median diameters between −5.5 and 0.2 ϕ (~45 mm–0.9 mm; Charbonnier et al., 2013). The valley-confined PDC deposits have thickness variations (from 3 to 14 m) that correspond to sudden changes in channel morphology and confinement (Charbonnier et al., 2013).

Deposits of the 5 November PDCs are generally rich in charred vegetation, which was originally composed mainly by evergreen angiosperm trees, herbs and shrubs (Sutomo and Fardila, 2013). Pieces

UNCORRECTED PROOF

Table 1
Charcoal reflectance data and related temperature estimates for each site.

Site	D (km)	Lithofacies	Lat (°S)	Long (°E)	G	MLRo% ± 1σ	MHRo% ± 1σ	L-T_{emp} (°C)	H-T_{emp} (°C)
212	2.1	U1 – L2	7° 33.544′	110° 27.292′	A	0.17 ± 0.04		240–284	
270	2.7	U1 – L1	7° 33.976′	110° 26.634′	A	0.41 ± 0.08		297–323	
235	2.8	U1 – L1	7° 33.731′	110° 27.752′	A	0.38 ± 0.05		290–320	
215	3.1	U1 – L1	7° 34.077′	110° 27.494′	B	0.74 ± 0.15		329–358	
271	3.1	U1 – L1	7° 34.181′	110° 26.679′	A	0.33 ± 0.09		278–315	
272	3.5	U1 – L1	7° 34.412′	110° 26.549′	A	0.25 ± 0.06		259–306	
417	3.7	U1 – L1	7° 34.480′	110° 27.370′	A	0.31 ± 0.03		274–306	
416	3.8	U1 – L1	7° 34.542′	110° 27.337′	A	0.33 ± 0.03		278–315	
338	3.9	U1 – L1	7° 34.619′	110° 26.570′	C	0.41 ± 0.12	1.12 ± 0.06	297–323	364–399
420	4.9	U1 – L1	7° 35.163′	110° 27.344′	C	0.28 ± 0.04	1.36 ± 0.19	266–309	386–444
469	4.9	U1 – L2	7° 35.111′	110° 27.554′	A	0.36 ± 0.03		285–318	
8	5.4	U1 – L1	7° 35.425′	110° 27.217′	A	0.36 ± 0.03		285–318	
326	5.7	U1 – L2	7° 35.621′	110° 26.496′	A	0.31 ± 0.03		273–312	
478	5.8	U1 – L1	7° 35.607′	110° 27.500′	C	0.25 ± 0.04	1.52 ± 0.22	259–306	401–458
488	5.8	U1 – L1	7° 35.654′	110° 27.078′	A	0.32 ± 0.02		276–313	
489	5.9	U1 – L1	7° 35.719′	110° 26.911′	A	0.37 ± 0.10		288–319	
463	6.2	U1 – L1	7° 35.766′	110° 27.689′	A	0.35 ± 0.02		283–316	
273	6.2	U1 – L1	7° 35.832′	110° 26.137′	B	0.59 ± 0.17		316–342	
276	6.2	U1 – L1	7° 35.846′	110° 26.119′	A	0.33 ± 0.04		278–315	
346	6.3	U1 – L2	7° 35.941′	110° 26.480′	A	0.33 ± 0.05		278–315	
493	6.4	U1 – L1	7° 35.998′	110° 26.843′	A	0.36 ± 0.03		285–318	
349	6.5	U1 – L2	7° 36.051′	110° 26.348′	A	0.25 ± 0.08		259–306	
352	6.7	U1 – L2	7° 36.122′	110° 26.380′	A	0.30 ± 0.04		271–311	
11-12	7.3	U1 – L1	7° 36.394′	110° 27.582′	C	0.36 ± 0.09	1.49 ± 0.26	285–318	398–456
433	7.3	U1 – L1	7° 36.477′	110° 27.141′	A	0.32 ± 0.04		276–313	
423	7.4	U1 – L1	7° 36.512′	110° 27.317′	A	0.35 ± 0.02		283–317	
249	13	Valley-confined	7° 39.694′	110° 27.802′	A	0.31 ± 0.06		274–312	
2241	13	Valley-confined	7° 39.718′	110° 27.834′	A	0.33 ± 0.03		278–315	
397	13	Valley-confined	7° 39.746′	110° 27.844′	A	0.34 ± 0.04		281–316	

D, runout distance from crater; *G*, samples group; *MLRo*% and *MHRo*% represent the mean low and high reflectance value, respectively; *L-T*$_{emp}$ and *H-T*$_{emp}$ represent the temperature of emplacement related to the *MLRo*% and *MHRo*%, respectively. Unit U1 and its layers L1 and L2 are the same ~~of~~ Komorowski et al., 2013. Temperatures are inferred from experimental curves by Scott and Glasspool (2005, 2007) and Ascough et al. (2010).

of charred branches and trunks (on the order of few centimeters) were collected in most of the analyzed deposits (Fig. 2). In the absence of macroscopic (>1 mm) charcoal pieces, bulk samples (sites 8, 326, 397, 417, 433) were collected directly from the matrix (Fig. 2). In these few cases, small fragments of charcoal were found dispersed within the matrix during laboratory analysis.

To examine the thermal evolution of the dominantly topography-mantling 5 November PDCs, sampling sites were selected in different topographic settings (i.e. ridge tops, interfluves and deep channels) across the impacted area, and at varying distances from the source (from ~2.1 to ~13.5 km). In particular, ten sites (212, 215, 417, 416, 420, 469, 8, 478, 463, 11–12) were sampled from deposits related to the topography-mantling PDCs that partially spilled over both the Kendil Ridge and the Gendol valley, and continued propagating southward along the Gendol-Woro interfluve. These samples were collected along a N – S transect at distances of ~2.1 to 7.3 km from the summit. One site (235) was located in deposits formed by topography-mantling PDC lobes in the east side of the Woro drainage (~2.8 km from the vent). Eight sites (270, 271, 272, 338, 326, 346, 349, 352) were sampled in the right side of the Opak river through a NE – SW transect ~4 km long. Here the deposits represent topography-mantling PDCs that detached from the main axial flow direction of the Gendol channel and overpassed a series of subparallel ridges (i.e. the western walls of the Gendol and Opak valleys), spreading onto the Kinarhejo area. Two sites (273, 276) were sampled from deposits situated at the southwest distal edge of the topography-mantling PDC impact area (~6.2 km from the volcano), where the flows stopped in the Kuning – Opak interfluve before entering the Boyong drainage. Five sites (488, 489, 493, 433, 423) represent the overbanking deposits that cover the Gendol-Opak interfluve. They are distributed along a N – S transect at increasing distances from the source (from about 5.7 to 7.4 km).

Charcoal fragments were incorporated in epoxy resin and wet-polished. Samples were not heated during preparation to prevent possible effects on the organic matter present. The polishing procedure was performed adopting grinding papers (grain size of 250, 500 and 1000 μm) and isopropanol lubricant. The samples were then polished with alumina powder of grain sizes from 1 to 0.01 μm. Samples were examined through a Zeiss Axioskop 40 microscope under oil of ne = 1.518 at about 23 °C, using an Epiplan–Neofluar 50× optics. The incident light source was a tungsten–halogen lamp (12 V, 100 W) filtered at 546 nm. Reflectance measurements (Ro%) were performed using the MPS 200 detection system by J&M Analytik AG in a dark-room. The instrument was calibrated with glass-NG1 (Ro% = 0%) and mono–crystalline standards of spinel (Ro% = 0.426), sapphire (Ro% = 0.595), yttrium-aluminum-garnet (Ro% = 0.905) and gadolinium-gallium-garnet (Ro% = 1.726) prior to the measurements. Calibration was repeated approximately every 2 h during the analysis using a group of three standards that were selected according to the Ro% range measured in the sample. Specimens were also photographed with a microscope–mounted Canon Power Shot G6. Up to 162 Ro% measurements were randomly selected within each sampling site in order to calculate the mean Ro% value and its standard deviation.

3. Results

A complete summary of the reflectance microscopy data for each site is provided in Table 1. In general, the majority of the collected plant material had a black color, leaving a black streak on hands and

UNCORRECTED PROOF

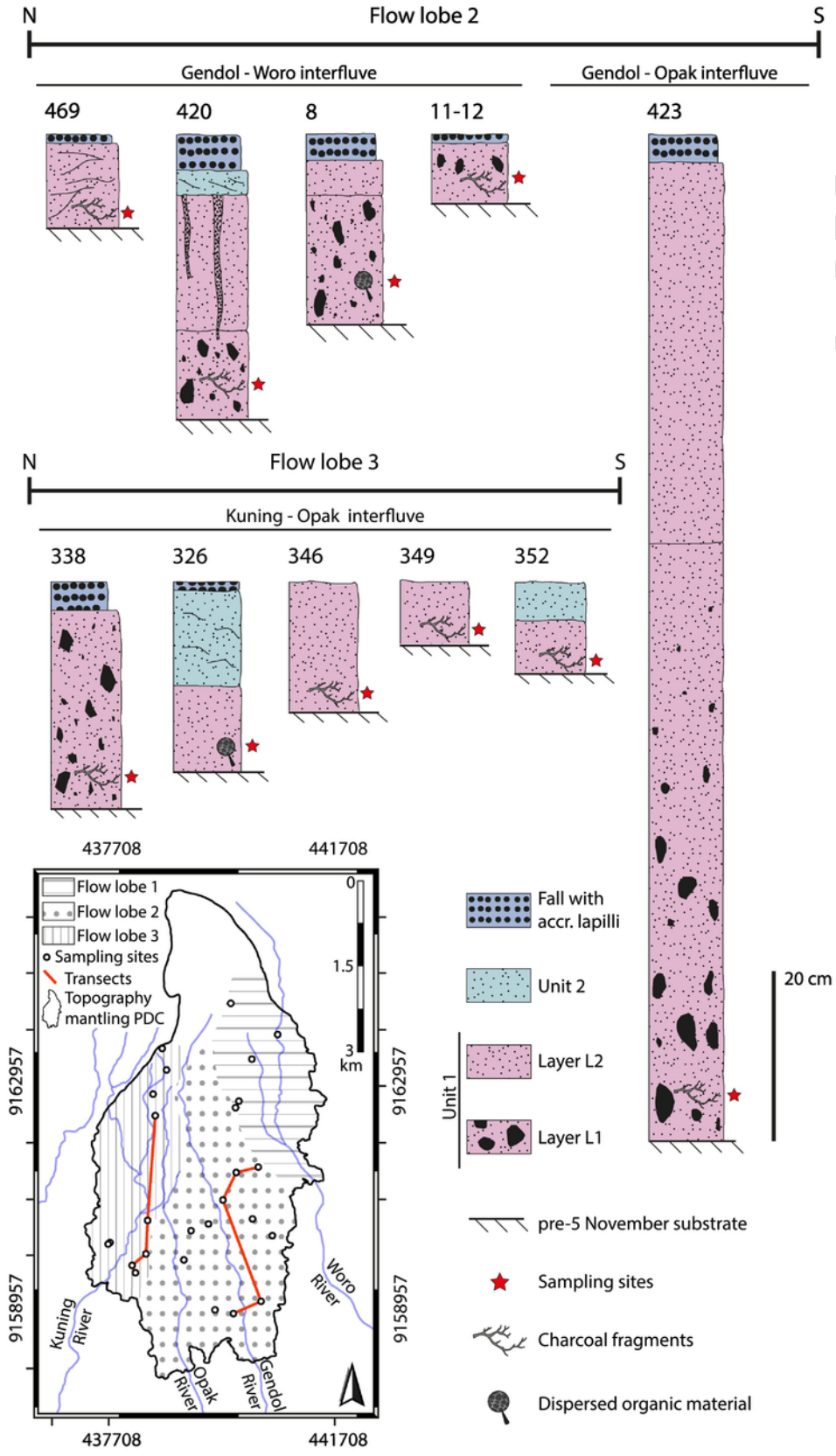


Fig. 2. Selected stratigraphic logs across the impact area of the topography-mantling PDC (refer to inset map for locations) modified after Komorowski et al. (2013), and position of the sampled charcoal fragments. In the absence of macroscopic (>1 mm) charcoal, dispersed organic material was found in bulk samples.

paper, and breaking easily under pressure. Under visible light microscopy, it also showed a varying degree of cell wall homogenization (i.e., loss of the original layering of the cell walls that results in a smooth, amorphous-appearing wall structure; see Scott, 2010), and could therefore be categorized as charcoal. All analyzed samples were homogeneously charred, since Ro% values are similar at the center and at the edge of the specimen. At one site (212), located in a very proximal region (~2.1 km) on top of the Kendil Ridge, the variety of colors of the sampled vegetation, ranging from brown/dark-brown to black-brown, indicated a range of conditions from uncharred to poorly charred, respectively. The uncharred branches and rootlets may still have been heated to a temperature of up to 200 °C, as below this value the reflectance cannot be measured (Scott and Jones, 1991).

Overall, partially and fully charred fragments were well-preserved within the 5 November PDC deposits at all localities, and their mean Ro% range from 0.17 ± 0.04% to 1.52 ± 0.22% (Fig. 3). Samples within each sampling site could be very homogeneous or show a scatter in Ro% values. Based on their cumulative frequency (i.e., the sum of the Ro% frequencies of all the samples within the same sampling site), we classify all sites into one of three groups (A, B, C). Group A sites are those showing a narrow and well-defined cumulative Gaussian distribution of reflectance values of all measured samples, with very small standard deviation (Fig. 4A–H). Group A sites represent 79% of all sites (n = 23; Table 1). Group A specimens are characterized by a poor homogenization of the cells and yield mean Ro% values that vary between 0.17 ± 0.04% and 0.41 ± 0.08%. Group A samples occur widely throughout the spatial extent of the topography-mantling PDC deposits (in both layers L1 and L2), regardless of their topographic location and their distance from the crater (Fig. 1). At distal localities, samples from valley-confined PDC deposits record the same degree of charring as observed in samples from proximal topography-mantling lithofacies.

Group B sites show a larger scatter in Ro% than that observed in Group A (Fig. 4I, J), suggesting that samples characterized by different Ro% values, and thus emplacement temperatures, are present in the same site. The mean cumulative Ro% values range from 0.59 ± 0.17% to 0.74 ± 0.15%. The cumulative frequency histograms show a high standard deviation, which may be due to the overlap of two Gaussian distributions that are difficult to separate. Group B sites (about 7%; Table 1) are found sporadically in layer L1 located in the Kuning (sample 273) and Woro (sample 215) rivers (Fig. 1).

Group C sites (about 14%, Table 1) are characterized by the presence of two main clusters of Ro% values identifiable by two distinct Gaussian distributions (Fig. 4K, L). Here, specimens coexist with both low and high homogenization of the cell structure, with mean Ro% ranging from 0.25 ± 0.04% to 0.41 ± 0.12%, and from 1.12 ± 0.06% to 1.52 ± 0.22%, respectively. Group C sites are found in layer L1 at few locations in the Gendol-Woro interfluve (samples 420, 478, 11–12) and in the Opak drainage (sample 338; Fig. 1).

4. Discussion

4.1. Determining the emplacement temperature of the 5 November PDC deposits

Here we use the experimental curves proposed by Scott and Glasspool (2005, 2007) and Ascough et al. (2010) to convert Ro% into temperature values. Scott and Glasspool (2005, 2007) performed a series of charring experiments using branches of *Sequoia sempervirens* to build an empirical Ro% vs temperature curve (Fig. 5). Experimental data from woods of *Pinus sylvestris* and *Rhizophora apiculate* were used by Ascough et al. (2010) to extrapolate a similar relationship. As discussed by Ascough et al. (2010) and Hudspith et al. (2010), no meaningful difference can be observed in Ro% values between angiosperms and gymnosperms for the same temperature conditions. Moreover, Scott and Glasspool (2007) showed that the experimental Ro% - T curve determined for the bracket fungus *Ganoderma* sp. lies close to that of the *Sequoia sempervirens*, although the former is not likely to contain lignin in its structural cells (Paterson, 2006). We therefore assume that these curves can be applied to our samples, which are most likely an ensemble of different angiosperms species,

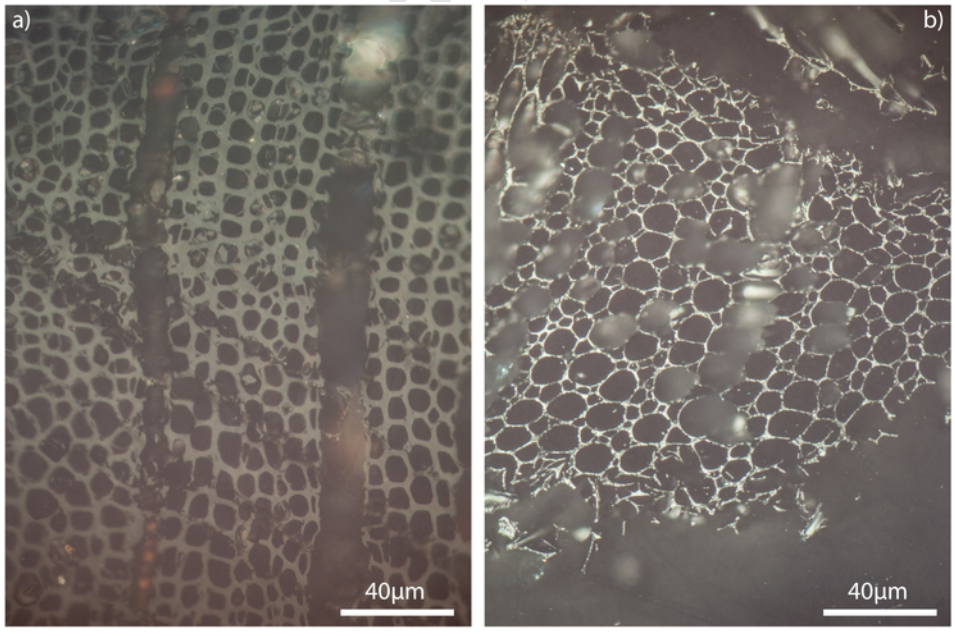


Fig. 3. Reflected light microphotographs of polished blocks under oil showing variable degree of charring. (a) Incompletely charred specimen (from site 270), as evidenced by the cell walls that are not completely homogenized (mean Ro% = 0.36). (b) Fully charred fragment (from site 338) with high homogenized cell walls yielding mean Ro% = 1.42.

PROOF

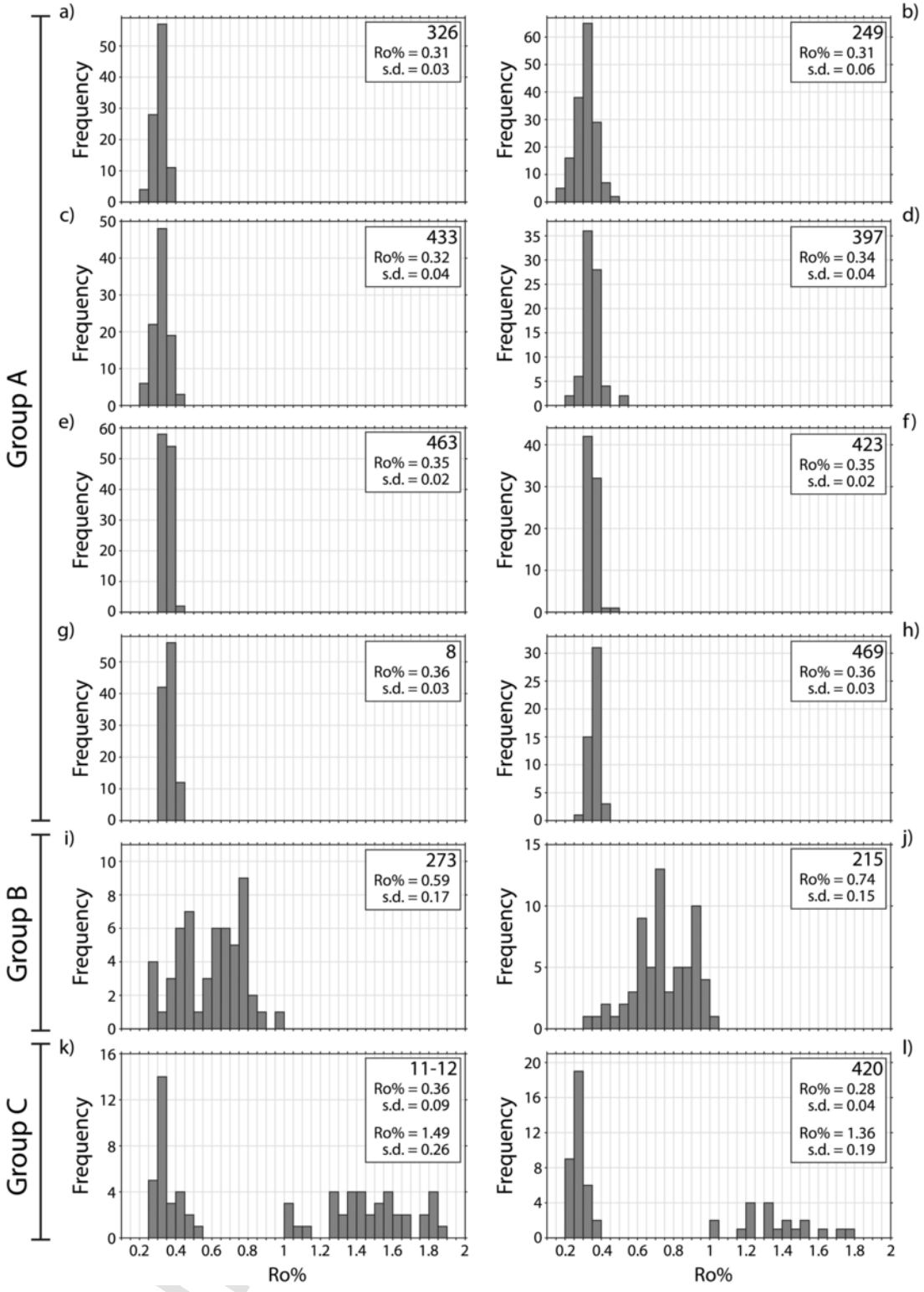


Fig. 4. Results of optical analyses are shown in terms of frequency histograms of Ro% values. Three groups have been identified. (a–h) Group A sites are those that show a well-defined cumulative Gaussian distribution in Ro% data, with very small standard deviation. (i–j) In sites of Group B, the cumulative Gaussian distribution is less defined because of the large variation in Ro% due to the overlap of different Ro% families. (k–l) Group C sites are those yielding a distinct bimodal pattern of Ro%. The mean Ro% values and standard deviations are reported in the inset of each sample.

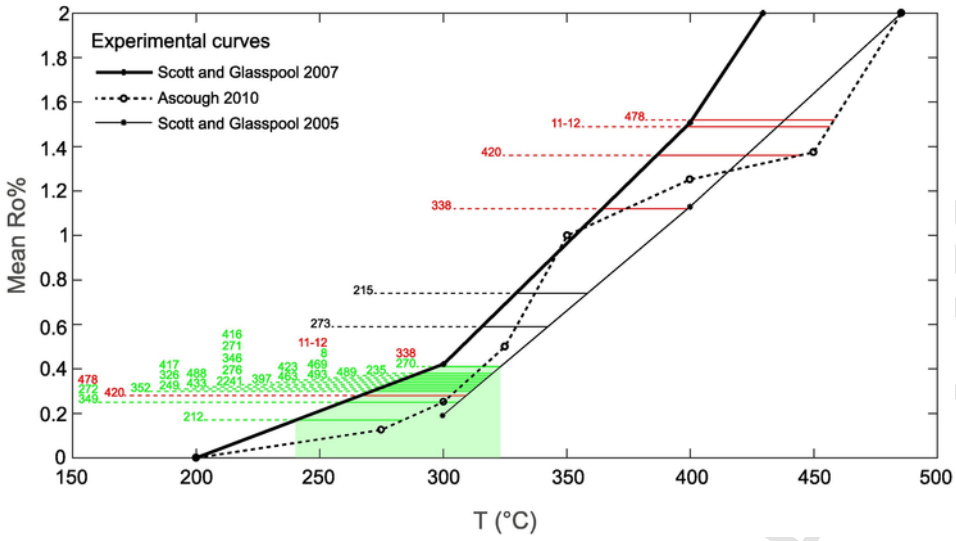


Fig. 5. Conversion of Ro% data into paleo-temperatures. Ro% values are converted into temperature values adopting the experimental curves for *Sequoia sempervirens* and *Pinus sylvestris*, after Scott and Glasspool (2005, 2007) and Ascough et al. (2010), respectively. For a given Ro% value, the temperature interval defined by the combination of these curves (experimental curves in legend) is assumed here as an estimate of the mean PDC emplacement temperature at that location. Green, black and red lines represent sites of Group A, B and C, respectively. The green shaded area indicates the minimum emplacement temperature for the 5 November PDC. (For interpretation of the references to color in this figure legend, the reader is referred to the web version of this article.)

although their taxonomical identification is outside the purpose of this paper. As a result of the differences in experimental procedures between the various studies, slightly different temperature values were obtained for a given Ro%. We use the range of temperatures defined by the combination of these curves as our best estimate of the PDC emplacement temperature (Fig. 5).

Our Ro% results clearly indicate that the largest proportion of the samples experienced the same degree of charring. Group A sites (79%) show well-clustered Ro% values in a narrow peak averaging at 0.32±0.04 yielding temperatures between 240 and 320 °C (green lines: Fig. 5). Group B sites (7%) show much more scattered and polymodal Ro% values averaging ~~at~~ 0.66±0.16, which translate into temperatures of emplacement of 316–358 °C (black lines: Fig. 5). Ro% data of Group C (14%) reveal the presence of two marked populations of charcoal materials in the same sampling site, where the population with the lowest mean values overlap with specimens of Group A and convert~~ed~~ ~~in~~ similar temperatures of 259–323 °C, whereas the highest Ro% values are very scattered and indicate temperatures of 364–456 °C (red lines: Fig. 5). We underline here the remarkable homogeneity of the Ro% values from specimens across the whole area of emplacement of the 5 November PDC deposit. Only Group B and Group C recorded also higher emplacement temperatures, along with the lower Ro% range recorded by Group A (Fig. 4). In order to interpret the polymodal distribution of the outlier Group B and Group C we must take into consideration the grainsize distribution and inherent thermal disequilibrium of dome collapse deposits. The ash-sized particles (<2 mm diameter) can be considered thermally and mechanically coupled within flow (e.g. Marble, 1970; Cerminara, 2015) and rather homogeneous in the deposit. Block-sized clasts (>64 mm), instead, have a much larger heat capacity and retain their initial temperature in the deposit for several hours/days (Bardot, 2000). We interpret the Ro% values of the main Group A (also present in Group B and Group C) as associated with specimens that have reached equilibrium within the surrounding ash matrix. We interpret the secondary higher Ro% values recorded by samples of Group B and C, which were found in the coarsest layer L1, as resulting from ~~a~~ proximity with large hotter block-sized clasts, rather than being related to a transient thermal history, since the reflectance values within the individual specimens are very similar and did not show a thermal gradient from the edge to the center. We therefore propose that the minimum emplacement temperature of the 5 November PDCs was between 240 and 320 °C (Fig. 5). These values are in excellent agreement with the temperature proposed by Jenkins et al. (2013) and Baxter et al. (2017) for the dilute detached PDCs in Bronggang village, directly adjacent to the valley-confined PDCs of sites 249, 2241 and 397. Site 212 is distinct because it contains some uncharred plants that were taken at the interface between the topography-mantling PDC deposit and the underlying soil, where the flow was probably being cooled by the erosive interaction with wet soil.

Given that several PDCs had occurred since October 26 and that they had already knocked down and charred part of the living vegetation, it may be argued that the previously formed charcoal could have been transported within the subsequent PDCs of 5 November, affecting its temperature estimation. However, it is important to note that the Ro% value of charred specimens is not reversible, but relates to the highest temperature experienced since it can be overprinted only by subsequent charring at higher temperatures (McParland et al., 2009). Assuming that some woody plants were reworked, this leads to two possible hypotheses. The first is that if the temperature of the 5 November PDCs was higher than those of PDCs generated during previous eruptions (e.g. 26 October directed explosion), our samples would have recorded the ~~thermal~~ overridden ~~of~~ the last event. On the other hand, if the 5 November PDCs were cooler, our proposed temperature may overestimate their actual thermal state. Regardless of which hypothesis is correct, it is important to emphasize that our data highlight a thermal signal that is homogeneously distributed across topography and it is far below magmatic temperatures. Eyewitness accounts, field observations and impact analysis indicate that most of the vegetation was not intensely charred by unconfined dilute PDCs resulting from the initial 26 October directed explosion and that temperatures were lower than those reached by the 5 November paroxysmal explosion (Jenkins et al., 2013; Komorowski et al., 2013).

UNCORRECTED PROOF

4.2. Thermal evolution of the 5 November PDCs

The charcoal data presented here indicate that the 5 November PDCs were emplaced over a wide area of contrasting topographic conditions maintaining a fairly homogeneous temperature, even though their dynamics constantly evolved along the flow path as a result of interaction with an irregular terrain morphology. Fig. 6 shows the inferred temperature values for each locality versus their distance from the volcano summit. From this figure, it is clear that there is no appreciable difference in the degree of charring across the entire deposit, nor between the distal valley-confined PDC deposits and the topography-mantling lithofacies. It is important to note that the little temperature variations observed across the lobes of the topography-mantling PDC deposits are well within the resolution of the method (inset in Fig. 6). The initial inferred temperature of ~900 °C (Erdmann et al., 2016; Preece et al., 2016) is ~600 °C hotter than the emplacement temperature of the PDC as it reached vegetated flanks, approximately 2 km from source.

Assessing the temperature of PDC deposits formed by dome collapse (i.e., block-and-ash flow deposits) is complicated by the fact that the extent of cooling of the lava carapace before it detaches from the lava dome is unknown. At the time of gravitational collapse, the outer margin of the dome could be hot, warm or even cold. As far as we know, temperatures of block-and-ash flow deposits may vary substantially, largely because they reflect the broad thermal range that is associated to the dome source materials (Uehara et al., 2015). Despite this possible thermal heterogeneity, block-and-ash flow deposits are generally found at high temperatures because of their typical high concentration and valley-confined behavior (Cole et al., 2002; Uehara et al., 2015; Voight and Davis, 2000). Voight and Davis (2000) inferred that the 1994 channeled coarse-grained block-and-ash flows at Merapi were emplaced at a temperature of about 550 °C, whereas detached dilute currents were below 200 °C, highlighting the efficiency of the heat exchange between the dilute ash-particle mixture and the external atmosphere. A similar result was obtained by Charbonnier and Gertisser (2008) who estimated 400 °C for the 2006 block-and-ash flow deposit and about 165 °C for the associated dilute PDC.

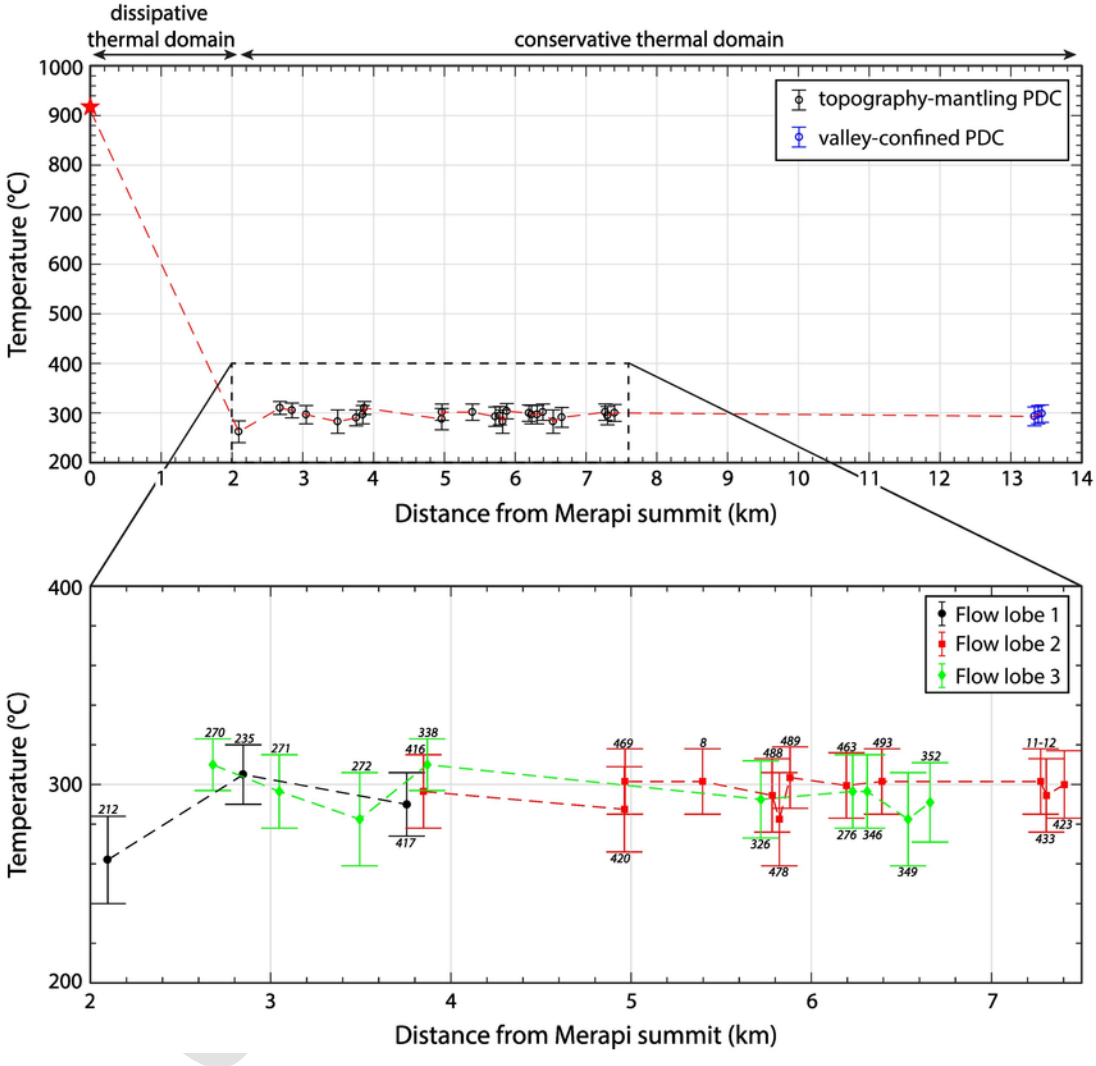


Fig. 6. Emplacement temperature variation as a function of the distance from source for the topography-mantling and co-genetic valley-confined PDC deposits of 5 November eruption. The red star marks the inferred initial temperature of the dome before the paroxysmal event as deduced from studies of the dome petrology and microtextures by Erdmann et al. (2016) and Preece et al. (2016). Inset plot shows an expanded view of the estimated temperatures of the topography-mantling PDC deposits. Colors refer to the main PDC flow lobes (see Fig. 1). Site numbers are in italics. (For interpretation of the references to color in this figure legend, the reader is referred to the web version of this article.)

The temperature of the PDC deposits produced during the 5 November 2010 paroxysmal activity at Merapi appears to have been unaffected by changes in flow concentration, i.e. between the topography-mantling and the valley-confined PDC (Fig. 6). Nevertheless, our temperature estimations are significantly lower than those that might be associated with hot dome-generated PDCs. The high magma extrusion rates estimated during 1–4 November (~25 $m^3 s^{-1}$; Pallister et al., 2013) suggest that the largest part of the dome that collapsed on 5 November was made of fresh magma, and therefore, its initial temperature was largely close to magmatic temperature. The temperatures evaluated at the time of the growth of the last crystals in the dome rock (i.e., the plagioclase microlites) have been estimated to range between 925 and 1000 °C (Erdmann et al., 2016; Preece et al., 2016). As a consequence, the thermal state of the associated PDCs should be much higher than that indicated by our data. Furthermore, the almost exclusive involvement of very dense vitric non-vesicular juvenile material in the PDC (~90% by weight, Komorowski et al., 2013) implies the presence of a considerable heat-source. All of these factors result in an extremely hot PDC at source. The logical first-order question is, therefore, which is the process (or processes) causing this significant temperature drop within the first two kilometers from source, i.e. along the upper slopes of the volcano? A first explanation is that efficient air ingestion during PDC propagation may have occurred as a result of topography effects in the proximal region (<2 km) (Fig. 7A). Cronin et al. (2013) and Komorowski et al. (2013) suggested that the combination of a very high initial mass eruption rate associated with the dome extrusion and collapse combined with the marked topographic features in the upper reaches of the Gendol valley, controlled the unusual and extreme mobility of the 5 November PDCs as well as their high dynamic pressures. Numerical experiments have evaluated the effects of volcano profiles on the flow dynamics of PDCs (Doronzo et al., 2012; Valentine et al., 2011). Model solutions show that the flow velocity, and in turn the degree of turbulence, is greatly dependent on the volcano slope angle. In the case considered here, the steep slope of the southern flank of Merapi (30–40°) has led to the rapid acceleration of the descending gas-particle mixture, which reached velocities of ~50–70 m/s before impacting the Gunung Kendil ridge (Kelfoun et al., 2017; Komorowski et al., 2013). The high degrees of turbulence generated by the high mixture velocity would have led to an intense turbulent mixing with the atmosphere (Fig. 7), reducing the density and temperature of the moving current (Doronzo et al., 2012; Valentine et al., 2011). At about 1.8 km away from the vent, the PDCs impacted the major transverse topographic ridge of Gunung Kendil (~240 m high), which forced most of the mass (~95% of the volume) to pass through the Gendol funnel constriction (Komorowski et al., 2013). After entering this canyon, the dynamics of the main PDCs were likely to be strongly constrained by the narrowing bottleneck at the base of the funnel, which reduced the flow accommodation space allowing the flow to expand vertically (Fig. 7). The vertical expansion of the sustained hot current spontaneously induced the formation of turbulent eddies that favored the rapid entrainment of cold atmospheric air and a dramatic decrease of the flow density and temperature. As the expanded and cooled current exited this constriction, its sudden collapse triggered the generation of rapidly-moving, highly-destructive, topography-mantling and relatively cold PDCs (Komorowski et al., 2013). At the same time, <10% of the total mass overpassed the Kendil ridge and continued propagating to the southeast in the Woro drainage system. It is likely that, in this sector, the lower mass content along with the extreme turbulence generated as a result of the impact against the ridge similarly favored a rapid cooling of the PDCs.

Pyroclastic mixtures may also have been rapidly cooled as a result of the dome explosion mechanism, where internal overpressure may have led to an initial blast-like process (Komorowski et al., 2013).

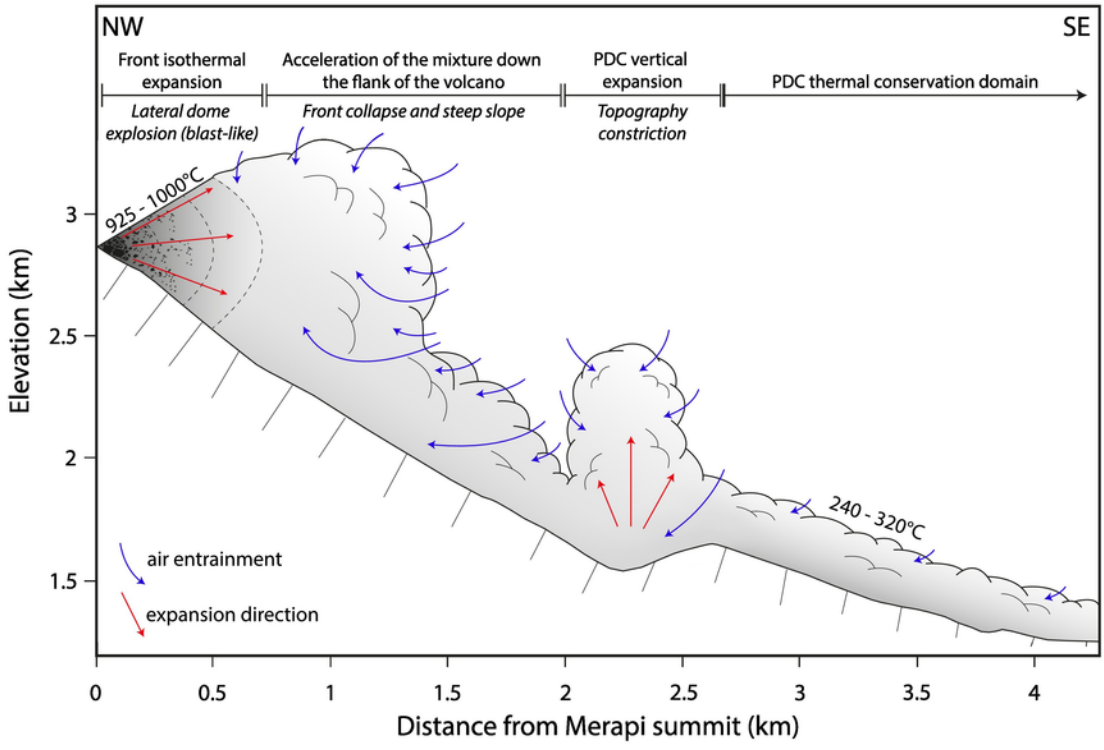


Fig. 7. Cartoon illustrating the inferred processes potentially responsible for the observed temperature drop. The illustrated processes do not need to have all occurred, and are intended to summarize the possible ways the PDC experienced an efficient air entrainment in proximal areas. The extension of the flow front and flow thickness is not to scale.

The initial expansion of the blast can be approximated as isothermal (i.e., burst phase; Esposti Ongaro et al., 2008, 2012). This approximation is reasonable because of the relatively large heat capacity of the pyroclasts and the small mass fraction of the gas phase, implying that such a mechanism cannot decrease the temperature of the pyroclasts. Numerical simulations have shown that the burst phase lasts at most a few seconds, after which the gravity exceeds the pressure forces leading to the collapse of the expanded mixture and generation of PDCs (Esposti Ongaro et al., 2008, 2012). We therefore propose that the possible role of the initial blast-phase is to provide an extensive collapse front and an expanded mixture for the efficient entrainment of cold air during the gravitational collapse-phase (Fig. 7). Furthermore, the sudden collapse of the mixture likely produced a high velocity PDC that continued to accelerate along the steep upper slope of the volcano, enhancing turbulence and in turn mixing with surrounding air (Doronzo et al., 2012; Valentine et al., 2011). Similar emplacement temperatures have also been recorded in other well-studied historical blast-generated PDC deposits such as the 18 May 1980 at Mt. St. Helens (96–325 °C; Banks and Hoblitt, 1996) and the 26 December 1997 at Soufrière Hills (300–425 °C; Scott et al., 2008).

Since we have only few distal temperatures for the valley-confined PDC deposits, we cannot exclude that upstream the valley-confined PDC could have been hotter. The upper valley-confined PDC deposits could have been fed by an undercurrent poorly or unaffected by the expansion generated by the channeling effect of the Gendol funnel. It is noteworthy, however, that the isolated fires caused by the dense overspill along the Gendol valley were interpreted by Jenkins et al. (2013) as due to the presence of high flammable items rather than very high temperatures.

It is clear that these interpretations should be tested numerically to provide more rigorous and quantitative information on the inferred source and transport mechanisms leading to effective cooling of the PDCs and increases in their mobility. Irrespective of the actual mechanisms, we show that there is a need for an initial very fast cooling process to justify the homogeneous low temperatures recorded by the 5 November PDCs beyond 2.1 km from vent.

Remarkably, after these very dissipative initial thermal domains, the 5 November topography-mantling PDC deposits maintained a nearly constant temperature until the edge of their depositional area (Fig. 6). As shown by Komorowski et al. (2013), once the PDCs passed the Gendol funnel and some irregular medial topographic profiles, they essentially flowed over a relatively smooth topography. Moreover, numerical simulations have suggested that the unusual power of the 5 November PDCs can be explained by a large mass flux that sustained the mass transfer from the concentrate to the dilute current (Kelfoun et al., 2017). It is likely that both of these conditions contributed to limiting the heat transfer between the flow and the external environment along the path, as the prolonged lateral mass flow rate and the topography-induced low turbulence limited the PDC transport system, or at least the basal part of the current from where hot particles settled, to entrain enough cold atmospheric air. As shown by experimental studies and numerical simulations, the development of vertical concentration and velocity gradients, and hence vertical turbulence gradients, inside a small volume PDC strongly affect the exchange physics both within the current itself (from the basal region to the suspended load in the upper part of the flow) and between the current and external environment (Benage et al., 2016; Breard and Lube, 2017; Breard et al., 2016). Thus, the efficiency of air entrainment varies significantly with height in the current, with the basal region that is subjected to moderate or limited entrainment (Benage et al., 2016). This also may explain why the emplacement temperature of the 5 November PDC deposits is maintained almost constant for several kilometers. We believe that once the expansion phase is exhausted, the subsequent collapsing phase results in small volume PDCs that are highly sustained in terms of mass preserving their temperature and destructive power, similar to more voluminous PDCs that form large-volume ignimbrites (Lesti et al., 2011; Trolese et al., 2017).

All of these observations have important implications in terms of hazards and risk assessment suggesting that PDCs can maintain lethal and damaging temperatures for exposed population and structures even on their edges and near their maximum runout, and thus near the edge of exclusion zones, as well exemplified in 2010 at Merapi (Jenkins et al., 2013; Baxter et al., 2017) and in 1997 at Soufrière Hills (Loughlin et al., 2002; Baxter et al., 2005).

5. Conclusion

We have presented reflectance data of charcoal fragments preserved within the PDC deposits emplaced during the 5 November 2010 event, the most disastrous volcanic eruption observed at Merapi since 1872. Reflectance data are mostly clustered in low values ranging from 0.17 ± 0.04% to 0.41 ± 0.08%, with few specimens yielding higher values suggesting a disequilibrium state of the deposits induced by hot bomb-size juvenile clasts. The lower values translate to minimum charring temperatures in the range of 240–320 °C, which are in good agreement with those previously estimated by Jenkins et al. (2013) and Baxter et al. (2017). These temperature data are ubiquitously distributed throughout most of the impact area of the paroxysmal PDCs, indicating that the flow transport system was unable to lower the transported thermal energy over emplacement distance. This is in spite of the fact that the flow evolved in its dynamics as it propagated over a complex terrain along the path. The high extrusion rates at which the dome that collapsed ~~of~~ 5 November was built during 1–4 November, as well as its very dense and vitric non-vesicular characteristics, suggest that the dome might not have cooled substantially and preserved high temperatures. The temperatures of the initial dome collapse PDCs were thus likely much higher (~600 °C) than those we have estimated. We propose that different causes may have contributed to this thermal discrepancy: the steep volcano upper slopes that favor PDC acceleration and air entrainment; the role of the valley constriction at the break in slope along the upper reaches of the Gendol valley, promoting rapid expansion of the gas-particle mixture and the transition from a concentrated valley-confined to a turbulent topography-mantling PDC; the possible blast-like expansion at source providing an extensive collapse front for efficient entrainment of cold atmospheric air. Since the temperature data presented here unequivocally need a mechanism to explain a very early and strong temperature drop, additional quantitative experimental investigations can tease apart the various hypotheses raised by this study. Moreover, these models will need to address the specific findings from this work describing possible mechanisms for the initial sharp temperature drop of the PDC soon after its inception and then quantifying its much slower decay for most of the PDC run-out thereafter. This has significant implications for the assessment of the thermal risk posed by PDCs to people and structures in their most distal runout area.

Acknowledgements

We are grateful to RISTEK for allowing us to undertake this research and to the Yogyakarta Special Territory for administrative support. We thank Dr. Surono, Dr. Hendrasto (PVMBG/CVGHM), and Dr. Subandryio (BPPTKG) for their steadfast support, and our Indonesian colleagues for field and administrative assistance. We are

UNCORRECTED PROOF

very grateful to J-P. Toutain and Etny at IRD for valuable assistance and institutional support. We are indebted to Sofie and her staff at PVMBG for help with administrative procedures. We would like to thank T. Esposti Ongaro, S. Charbonnier, R. Gertisser, K. Preece and our DOMERAPI ANR colleagues for many constructive discussions. We thank the CASAVA (ANR-09-RISK-002), MIA-VITA (EU FP7-ENV contract 211393), DOMERAPI (ANR-12-BS06-0012) for partial support of this work for geological field work and sampling. We thank Domenico Doronzo and an anonymous reviewer for their thorough reviews and constructive suggestions that greatly improved the manuscript, and Joan Martí for handling the submission.

References

Ascough, P.L., Bird, M.I., Scott, A.C., Collinson, M.E., Cohen-Ofri, I., Snape, C.E., Le Manquais, K., 2010. Charcoal reflectance measurements: implications for structural characterization and assessment of diagenetic alteration. J. Archaeol. Sci. 37, 1590–1599. https://doi.org/10.1016/j.jas.2010.01.020.

Banks, N.G., Hoblitt, R.P., 1996. Direct temperature measurements of deposits, Mount St. Helens, Washington, 1980–1981. U.S. Geol. Survey Prof. Paper 1387, 1–76.

Bardot, L., 2000. Emplacement temperature determinations of proximal pyroclastic deposits on Santorini, Greece, and their implications. Bull. Volcanol. 61, 450–467. https://doi.org/10.1007/PL00008911.

Baxter, P.J., Boyle, R., Cole, P., Neri, A., Spence, R., Zuccaro, G., 2005. The impacts of pyroclastic surges on buildings at the eruption of the Soufrière Hills volcano, Montserrat. Bull. Volcanol. 67, 292–313. https://doi.org/10.1007/s00445-004-0365-7.

Baxter, P.J., Jenkins, S., Rosadi, S., Komorowski, J.-C., Dunn, K., Purser, D., Voight, B., Shelley, I., 2017. Human survival in volcanic eruptions: thermal injuries in pyroclastic surges, their causes, prognosis and emergency management. Burns https://doi.org/10.1016/j.burns.2017.01.025.

Benage, M.C., Dufek, J., Mothes, P.A., 2016. Quantifying entrainment in pyroclastic density currents from the Tungurahua eruption, Ecuador: integrating field proxies with numerical simulations. Geophys. Res. Lett. 43, 6932–6941. https://doi.org/10.1002/2016GL069527.

Breard, E.C.P., Lube, G., 2017. Inside pyroclastic density currents – uncovering the enigmatic flow structure and transport behaviour in large-scale experiments. Earth Planet. Sci. Lett. 458, 22–36. https://doi.org/10.1016/j.epsl.2016.10.016.

Breard, E.C.P., Lube, G., Jones, J.R., Dufek, J., Cronin, S.J., Valentine, G.A., Moebis, A., 2016. Coupling of turbulent and non-turbulent flow regimes within pyroclastic density currents. Nat. Geosci. 9, 767. https://doi.org/10.1038/ngeo2794.

Caricchi, C., Vona, A., Corrado, S., Giordano, G., Romano, C., 2014. 79AD Vesuvius PDC deposits' temperatures inferred from optical analysis on woods charred in-situ in the Villa dei Papiri at Herculaneum (Italy). J. Volcanol. Geotherm. Res. 289, 14–25. https://doi.org/10.1016/j.jvolgeores.2014.10.016.

Cerminara, M., 2015. The Multiphase Buoyant Plume Solution of the Dusty Gas Model. arXiv Prepr. arXiv. 1506, 01638.

Charbonnier, S.J., Gertisser, R., 2008. Field observations and surface characteristics of pristine block-and-ash flow deposits from the 2006 eruption of Merapi volcano, Java, Indonesia. J. Volcanol. Geotherm. Res. 177, 971–982. https://doi.org/10.1016/j.jvolgeores.2008.07.008.

Charbonnier, S.J., Germa, A.M., Connor, C.B., Gertisser, R., Preece, K., Komorowski, J.-C., Lavigne, F., Dixon, T.H., Connor, L.J., 2013. Evaluation of the impact of the 2010 pyroclastic density currents at Merapi volcano from high-resolution satellite imagery, field investigations and numerical simulations. J. Volcanol. Geotherm. Res. 261, 295–315. https://doi.org/10.1016/j.jvolgeores.2012.12.021.

Clarke, A.B., Voight, B., 2000. Pyroclastic current dynamic pressure from aerodynamics of tree or pole blow-down. J. Volcanol. Geotherm. Res. 100, 395–412. https://doi.org/10.1016/S0377-0273(00)00148-7.

Cole, P.D., Calder, E.S., Sparks, R.S.J., Clarke, A.B., Druitt, T.H., Young, S.R., Herd, R.A., Harford, C.L., Norton, G.E., 2002. Deposits from dome-collapse and fountain-collapse pyroclastic flows at Soufrière Hills Volcano, Montserrat. Geol. Soc. London, Mem. 21, 231–262. https://doi.org/10.1144/GSL.MEM.2002.021.01.11.

Correia, M., Maury, R., Arai, F., 1974. Mesure par leur pouvoir réflecteur, des températures de carbonisation des bois fossilisés dans les formations volcanique. Bull. Cent. Rech. Pau. 8, 527–536.

Cronin, S.J., Lube, G., Dayudi, D.S., Sumarti, S., Subrandiyo, S., Surono, 2013. Insights into the October – November 2010 Gunung Merapi eruption (Central Java, Indonesia) from the stratigraphy, volume and characteristics of its pyroclastic deposits. J. Volcanol. Geotherm. Res. 261, 244–259. https://doi.org/10.1016/j.jvolgeores.2013.01.005.

Doronzo, D.M., Martí, J., Sulpizio, R., Dellino, P., 2012. Aerodynamics of stratovolcanoes during multiphase processes. J. Geophys. Res. Solid Earth 117, https://doi.org/10.1029/2011JB008769.

Erdmann, S., Martel, C., Pichavant, M., Bourdier, J.-L., Champallier, R., Komorowski, J.-C., Cholik, N., 2016. Constraints from phase equilibrium experiments on pre-eruptive storage conditions in mixed magma systems: a case study on crystal-rich basaltic andesites from Mount Merapi, Indonesia. J. Petrol. 57, 535–550. https://doi.org/10.1093/petrology/egw019.

Esposti Ongaro, T., Neri, A., Menconi, G., De'Michieli Vitturi, M., Marianelli, P., Cavazzoni, C., Erbacci, G., Baxter, P.J., 2008. Transient 3D numerical simulations of column collapse and pyroclastic density current scenarios at Vesuvius. J. Volcanol. Geotherm. Res. 178, 378–396. https://doi.org/10.1016/j.jvolgeores.2008.06.036.

Esposti Ongaro, T., Clarke, A.B., Voight, B., Neri, A., Widiwijayanti, C., 2012. Multiphase flow dynamics of pyroclastic density currents during the May 18, 1980 lateral blast of Mount St. Helens. J. Geophys. Res. Solid Earth 117, 1–22. https://doi.org/10.1029/2011JB009081.

Genareau, K., Cronin, S.J., Lube, G., 2015. Effects of volatile behaviour on dome collapse and resultant pyroclastic surge dynamics: Gunung Merapi 2010 eruption. Geol. Soc. London, Special Publications 410, 199–218. https://doi.org/10.1144/SP410.6.

Hudspith, V.A., Scott, A.C., Wilson, C.J.N., Collinson, M.E., 2010. Charring of woods by volcanic processes: an example from the Taupo ignimbrite, New Zealand. Palaeogeogr. Palaeoclimatol. Palaeoecol. 291, 40–51. https://doi.org/10.1016/j.palaeo.2009.06.036.

Jenkins, S., Komorowski, J.-C., Baxter, P.J., Spence, R., Picquout, A., Lavigne, F., Surono, 2013. The Merapi 2010 eruption: an interdisciplinary impact assessment methodology for studying pyroclastic density current dynamics. J. Volcanol. Geotherm. Res. 261, 316–329. https://doi.org/10.1016/j.jvolgeores.2013.02.012.

Kelfoun, K., Legros, F., Gourgaud, A., 2000. A statistical study of trees damaged by the 22 November 1994 eruption of Merapi volcano (Java, Indonesia): relationships between ash-cloud surges and block-and-ash flows. J. Volcanol. Geotherm. Res. 100, 379–393. https://doi.org/10.1016/S0377-0273(00)00147-5.

Kelfoun, K., Gueugneau, V., Komorowski, J.-C., Aisyah, N., Cholik, N., Merciecca, C., 2017. Simulation of block-and-ash flows and ash-cloud surges of the 2010 eruption of Merapi volcano with a two-layer model. J. Geophys. Res. Solid Earth 122, 4277–4292. https://doi.org/10.1002/2017JB013981.

Komorowski, J.-C., Jenkins, S., Baxter, P.J., Picquout, A., Lavigne, F., Charbonnier, S., Gertisser, R., Preece, K., Cholik, N., Budi-Santoso, A., Surono, 2013. Paroxysmal dome explosion during the Merapi 2010 eruption: processes and facies relationships of associated high-energy pyroclastic density currents. J. Volcanol. Geotherm. Res. 261, 260–294. https://doi.org/10.1016/j.jvolgeores.2013.01.007.

Lesti, C., Porreca, M., Giordano, G., Mattei, M., Cas, R.A.F., Wright, H.M.N., Folkes, C.B., Viramonte, J., 2011. High-temperature emplacement of the Cerro Galán and Toconquis group ignimbrites (Puna plateau, NW Argentina) determined by TRM analyses. Bull. Volcanol. 73, 1535–1565. https://doi.org/10.1007/s00445-011-0536-2.

Loughlin, S.C., Baxter, P.J., Aspinall, W.P., Darroux, B., Harfpord, C., Miller, A.D., 2002. Eyewitness accounts of the 25 June 1997 pyroclastic flows and surges at Soufrière Hills Volcano, Montserrat, and implications for disaster mitigation. Geol. Soc. London, Mem. 21, 211–230. https://doi.org/10.1144/GSL.MEM.2002.021.01.10.

Marble, F.E., 1970. Dynamics of dusty gases. Annu. Rev. Fluid Mech. 2, 397–446.

McParland, L.C., Collinson, M.E., Scott, A.C., Campbell, G., 2009. The use of reflectance values for the interpretation of natural and anthropogenic charcoal assemblages. Archaeol. Anthropol. Sci. 1, 249–261. https://doi.org/10.1007/s12520-009-0018-z.

Surono, Jousset, P., Pallister, J., Boichu, M., Buongiorno, M.F., Budisantoso, A., Costa, F., Andreastuti, S., Prata, F., Schneider, D., Lieven, C., Humaida, H., Sumarti, S., Bignami, C., Griswold, J., Carn, S., Oppenheimer, C., Lavigne, F., 2012. The 2010 explosive eruption of Java's Merapi volcano—a "100-year" event. J. Volcanol. Geotherm. Res. 241, 121–135. https://doi.org/10.1016/j.jvolgeores.2012.06.018.

Pallister, J.S., Schneider, D.J., Griswold, J.P., Keeler, R.H., Burton, W.C., Noyles, C., Newhall, C.G., Ratdomopurbo, A., 2013. Merapi 2010 eruption—chronology and extrusion rates monitored with satellite radar and used in eruption forecasting. J. Volcanol. Geotherm. Res. 261, 144–152. https://doi.org/10.1016/j.jvolgeores.2012.07.012.

Paterson, R.R.M., 2006. Ganoderma – a therapeutic fungal biofactory. Phytochemistry 67 (18), 1985–2001. https://doi.org/10.1016/j.phytochem.2006.07.004.

Pensa, A., Porreca, M., Corrado, S., Giordano, G., Cas, R., 2015. Calibrating the pTRM and charcoal reflectance (Ro%) methods to determine the emplacement temperature of ignimbrites: Fogo A sequence, São Miguel, Azores, Portugal, as a case study. Bull. Volcanol. 77 (18)https://doi.org/10.1007/s00445-015-0904-4.

Preece, K., Gertisser, R., Barclay, J., Charbonnier, S.J., Komorowski, J.-C., Herd, R.A., 2016. Transitions between explosive and effusive phases during the cataclysmic 2010 eruption of Merapi volcano, Java, Indonesia. Bull. Volcanol. 78 (54)https://doi.org/10.1007/s00445-016-1046-z.

Scott, A.C., 2010. Charcoal recognition, taphonomy and uses in palaeoenvironmental analysis. Palaeogeogr. Palaeoclimatol. Palaeoecol. 291, 11–39. https://doi.org/10.1016/j.palaeo.2009.12.012.

UNCORRECTED PROOF

Scott, A.C., Glasspool, I.J., 2005. Charcoal reflectance as a proxy for the emplacement temperature of pyroclastic flow deposits. Geology 33, 589–592. https://doi.org/10.1130/G21474.1.

Scott, A.C., Glasspool, I.J., 2007. Observations and experiments on the origin and formation of inertinite group macerals. Int. J. Coal Geol. 70, 43–66. https://doi.org/10.1016/j.coal.2006.02.009.

Scott, A.C., Jones, T.P., 1991. Microscopical observations of recent and fossil charcoal. Microsc. Anal. 24, 13–15.

Scott, A.C., Sparks, R.S.J., Bull, I.D., Knicker, H., Evershed, R.P., 2008. Temperature proxy data and their significance for the understanding of pyroclastic density currents. Geology 36, 143–146. https://doi.org/10.1130/G24439A.1.

Sutomo, S., Fardila, D., 2013. Floristic composition of groundcover vegetation after the 2010 pyroclastic fire on Mount Merapi. J. Manajemen Hutan Tropika 19 (2), 85–93. https://doi.org/10.7226/jtfm.19.2.85.

Trolese, M., Giordano, G., Cifelli, F., Winkler, A., Mattei, M., 2017. Forced transport of thermal energy in magmatic and phreatomagmatic large volume ignimbrites: paleomagnetic evidence from the Colli Albani volcano, Italy. Earth Planet. Sci. Lett. 478, 179–191. https://doi.org/10.1016/j.epsl.2017.09.004.

Uehara, D., Cas, R.A.F., Folkes, C., Takarada, S., Oda, H., Porreca, M., 2015. Using thermal remanent magnetisation (TRM) to distinguish block and ash flow and debris flow deposits, and to estimate their emplacement temperature: 1991–1995 lava dome eruption at Mt. Unzen volcano, Japan. J. Volcanol. Geotherm. Res. 303, 92–111. https://doi.org/10.1016/j.jvolgeores.2015.07.019.

Valentine, G.A., Doronzo, D.M., Dellino, P., de Tullio, M.D., 2011. Effects of volcano profile on dilute pyroclastic density currents: numerical simulations. Geology 39, 947–950. https://doi.org/10.1130/G31936.1.

Voight, B., Davis, M.J., 2000. Emplacement temperatures of the November 22, 1994 nuée ardente deposits, Merapi Volcano, Java. J. Volcanol. Geotherm. Res. 100, 371–377. https://doi.org/10.1016/S0377-0273(00)00146-3.

UNCORRECTED PROOF